

Noncontact Haptic Rendering of Static Contact with Convex Surface Using Circular Movement of Ultrasound Focus on a Finger Pad

Tao Morisaki, Masahiro Fujiwara, *Member, IEEE* Yasutoshi Makino, and Hiroyuki Shinoda, *Member, IEEE*

Abstract—A noncontact tactile stimulus can be presented by focusing airborne ultrasound on the human skin. Focused ultrasound has recently been reported to produce not only vibration but also static pressure sensation on the palm by modulating the sound pressure distribution at a low frequency. This finding expands the potential for tactile rendering in ultrasound haptics as static pressure sensation is perceived with a high spatial resolution. In this study, we verified that focused ultrasound can render a static pressure sensation associated with contact with a small convex surface on a finger pad. This static contact rendering enables noncontact tactile reproduction of a fine uneven surface using ultrasound. In the experiments, four ultrasound foci were simultaneously and circularly rotated on a finger pad at 5 Hz. When the orbit radius was 3 mm, vibration and focal movements were barely perceptible, and the stimulus was perceived as static pressure. Moreover, under the condition, the pressure sensation rendered a contact with a small convex surface with a radius of 2 mm. The perceived intensity of the static contact sensation was equivalent to a physical contact force of 0.24 N on average, which was 12 times the radiation force physically applied to the skin.

Index Terms—Static contact sensation, convex surface, midair haptics, focused ultrasound.

I. INTRODUCTION

AIRBORNE ultrasound tactile display (AUTD), which can present a noncontact tactile stimulus, is a promising tool for haptics since it does not require users to physically contact with any devices [1]. An AUTD is a device with an array of independently controllable ultrasound transducers [2], [3], [4]. AUTDs can focus ultrasound waves on arbitrary points in the air by controlling the phase of each transducer. At the focus, a nonnegative force called acoustic radiation force is generated [5], which conveys a noncontact tactile stimulus onto human skin. This has been used in various applications [1], such as human motion guidance [6], [7], [8], touchable midair image displays [9], [10], [11], and remote visual-haptic communication system [12], as the noncontact stimulus by AUTD does not obstruct a user's movement and vision.

Recently, Morisaki et al. reported that AUTD can present not only vibratory sensations but also static pressure sensations [13]. A static pressure sensation is indispensable for

tactile displays because the sensation is the main component of contact perception and is perceived with a higher resolution than vibratory sensations [14]. However, in the conventional ultrasound haptics technique, a static pressure sensation is excluded from the presentable sensation of the AUTD. Ultrasound radiation force must be spatiotemporally modulated as it is less than several tens of mN [15], [16], [17], [18], [19]. This modulation has limited the tactile stimulus presented by the AUTD to a vibratory sensation. Morisaki et al. addressed this limitation and found that AUTD can present a static pressure sensation by repeatedly moving an ultrasound focus along the human skin at 5 Hz with a 0.2 mm spatial step width of the focus movement [13]. The focal trajectory was a 6 mm line, and the presentation location was a palm only.

In this study, we experimentally demonstrate that static pressure sensation by ultrasound can be evoked even at a finger pad. Moreover, we also show that by using a circular focal trajectory, the pressure sensation can render a static contact with a small convex surface on the finger pad. The radius of the rendered convex surface is varied from 2 to 4 mm. Rendering static contact with such a small convex surface has been difficult for conventional ultrasound haptics techniques because the perceptual resolution of vibratory sensations is lower than that of static pressure sensations [14]. This contact sensation rendering enables the noncontact tactile reproduction of fine corrugated surfaces with a minimal spot size of several millimeters, which is equivalent to a spatial resolution of 1 cm. Previous studies rendered an uneven surface (e.g., bumps and holes) using ultrasound. However, in these studies, the contact sensation was not static as the finger and palm must be moved to perceive the rendered surface. Howard et al. and Somei et al. rendered an uneven surface by dynamically changing the intensity or position of the ultrasound focus according to hand movement [20], [21].

In the experiment, an ultrasound focus rotating in a circle at 5 Hz is presented to a finger pad, and the radius of the trajectory is varied from 2 to 6 mm. We evaluate the intensity of the vibratory and movement sensations of the focus produced by the presented stimulus. We also evaluated curvature of the tactile shape (i.e., flat, convex, or concave) perceived on the finger pad. Moreover, we examine the optimal ultrasound focus shape for creating a perfect static pressure sensation.

Manuscript received xx; revised xx.

This work was supported in part by JSPS KAKENHI Grant Number 21J12305 and JST CREST JPMJCR18A2.

The authors are with the Graduate School of Frontier Sciences, the University of Tokyo, Kashiwa-shi, Chiba, 277-8561, Japan (e-mail: morisaki@hapis.k.u-tokyo.ac.jp; Masahiro_Fujiwara@ipc.i.u-tokyo.ac.jp; yasutoshi_makino@k.u-tokyo.ac.jp; hiroyuki_shinoda@k.u-tokyo.ac.jp).

II. RELATED WORKS

In this section, we summarize previous studies on point stimulation and haptic shape rendering using ultrasound to clarify the contribution of this study.

A. Vibratory and Static Pressure Sensation by Ultrasound

Two presentation methods have been employed to create a single point vibrotactile sensation: Amplitude Modulation (AM) [16] and Lateral Modulation (LM) [17], [18]. AM is a stimulation method wherein the amplitude of the presented radiation pressure is temporally modulated [16]. In LM, a vibratory stimulus is presented by periodically moving a single stimulus point (ultrasound focus) along the skin surface with constant pressure [17], [18]. Takahashi et al. presented an LM stimulus on the palm and showed that its perceptual threshold was lower than that of the AM stimulus [17], [18]. The focal trajectory used by Takahashi et al. was a line and circle with representative lengths of a few millimeters. Additionally, Spatiotemporal Modulation (STM) method have been used to create a larger trajectory of a moving focus [19], [22]. Frier et al. presented a circular STM stimulus with circumferences of 4–10 cm, which were larger than that of the LM stimulus presented by Takahashi et al [19], [17], [18].

A static pressure sensation can be produced by a low-frequency LM stimulus with a fine spatial step width of the focal movement. Morisaki et al. presented a static pressure sensation using an LM stimulus at 5 Hz with a step width of 0.2 mm [13]. The focal trajectory was a 6 mm line. Under this condition, the vibratory sensation included in the LM stimulus was suppressed to 5% in a subjective measure, and the perceived intensity was comparable to 0.21 N physical pushing force on average. The pressure sensation by ultrasound has been presented only on the palm, and whether the pressure sensation can be evoked on a finger pad has not been confirmed. This study aims to present the static pressure sensation to a finger pad. Morisaki et al. and Somei et al. presented a low frequency-fine step LM stimulus to a finger pad. However, they did not evaluate its tactile feeling [11], [21].

B. Rendering Haptic Shape Using Ultrasound

Several studies have presented symbolic two-dimensional haptic shapes, such as a line and circle on the palm using AUTD. To render them, Korres and Eid used AM with multiple foci [23]. Marti et al. and Hajas et al. used STM stimulus, wherein the focal trajectory is the perimeter of the target shape [24], [25]. Mulot et al. drew a curved line to the palm using STM stimulus and evaluated whether its curvature can be discriminated [26], [27].

Moreover, AUTD has been used for tactile reproduction of contact between 3D objects and hands. Inoue et al. presented a 3D static haptic image using an ultrasound standing wave [28]. Long et al. presented multiple ultrasound foci on a palm and rendered the contact shape with a virtual 3D object [29]. Matsubayashi calculated the contact area between a finger and a virtual 3D object and rendered this area to a finger

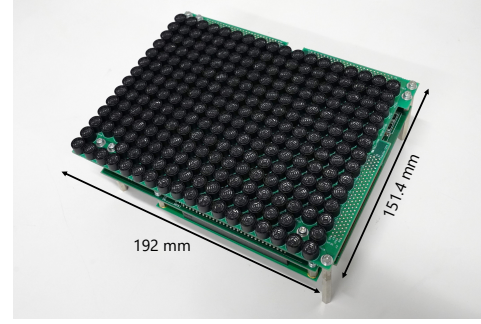


Fig. 1. One unit of airborne ultrasound tactile display (AUTD) used in this study. The one AUTD unit is equipped with 249 ultrasound transducers operating at 40 kHz.

pad by presenting an LM stimulus whose focal trajectory was the perimeter of the calculated contact area [30], [31]. These studies aimed to reproduce the macroscopic shape of a 3D object and did not reproduce contact shape with a fingertip-sized small convex surface, as in this study. Moreover, static pressure sensations were not presented in these studies. Long et al. used AM at 200 Hz [29] and Matsubayashi et al. LM at 100 Hz [30], [31]. The static haptic image presented by Inoue et al. was not modulated, but the participants had to keep moving their hands to perceive its tactile sensations [28].

Several studies have reproduced uneven surfaces using AUTD. Howard et al. presented three tactile shapes to a palm: bump, hole, and flat, by dynamically changing the intensity of the ultrasound focus based on the hand position [20]. Somei et al. presented a convex surface sensation to a finger pad by changing the position of the ultrasound tactile stimulus according to finger position [21]. Perceiving tactile shapes using these methods require active finger or hand movement. However, this study aims to perceive a static convex shape while the fingers are stationary.

III. AIRBORNE ULTRASOUND TACTILE DISPLAY (AUTD)

In this study, we used Airborne Ultrasound Tactile Display (AUTD) to present noncontact tactile stimuli. AUTD comprises an array of ultrasound transducers [2], [3], [4]. An AUTD can focus ultrasound by controlling a phase of each transducer, and focused ultrasound generates a nonnegative pressure called acoustic radiation pressure. Ultrasound focus can be narrowed to the diffraction limit.

Four AUTDs were used in the experiments. The one AUTD unit was equipped with 249 ultrasound transducers operating at 40 kHz (TA4010A1, NIPPON CERAMIC Co., Ltd.) [32], [33]. Fig. 1 shows the AUTD. Each AUTD communicated via the EtherCat protocol and was synchronously driven.

IV. STIMULUS DESIGN

A. Overview

In this section, we propose and describe two stimulus methods: LM-single focus (LM-S) and LM-multi foci (LM-M). In the subject experiment, we compared and evaluated them to investigate whether they could render a static contact sensation with convex surface. Fig. 2 shows a schematic of

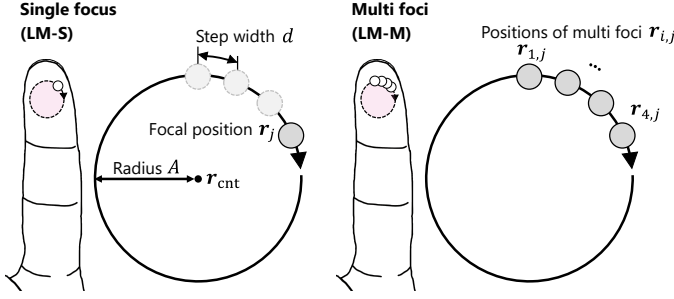


Fig. 2. Schematic of LM-S (single focus) stimulus and LM-M (multi foci) stimulus. In the LM-S, a single focus is periodically moved in a circle on a finger pad. In the LM-M, multiple foci are simultaneously rotated. The foci are placed along with the circular trajectory.

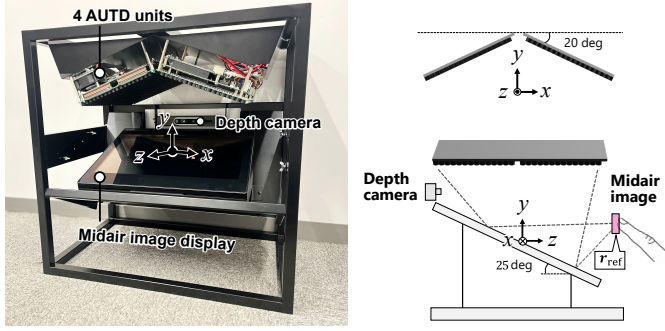


Fig. 3. Experimental equipment used in all subject experiments in this study. This equipment presents a midair image marker. An ultrasound tactile stimulus (LM stimulus) is presented when the finger of a participant touches this marker. The image marker was used to indicate a finger position to a participant.

these stimulus methods. In LM-S, a single ultrasound focus is periodically moved in a circle on the finger pad. The LM-S has been used in previous studies [19], [18], [30]; however, these studies have not evaluated whether this stimulus can produce static pressure and static contact sensations. In the LM-M stimulus, multiple ultrasound foci were simultaneously presented and periodically moved in a circle. The foci were placed along the circular focal trajectory so that they were in close proximity. The distance between foci d was fixed at 3 mm in the experiments.

In the experiments, the amplitude of each transducer was set to maximum and the driving phase for presenting the LM-M stimulus was calculated using a linear synthesis scheme. Let $\phi_i \in \mathbb{R}^{N_{\text{trans}}}$ be the phase for presenting each focus in the LM-M, and the phase for simultaneously presenting multiple foci $\phi \in \mathbb{R}^{N_{\text{trans}}}$ is expressed as follows:

$$\phi = \sum_{i=1}^{N_{\text{focus}}} \phi_i, \quad (1)$$

where $i \in \{1, \dots, N_{\text{focus}}\}$ is the index number of multiple foci, N_{focus} is the total number of multiple foci, and N_{trans} is the total number of transducers.

B. Formulation

First, we formulated a focus movement for the LM-S stimulus. The focus position in LM-S $\mathbf{r}_j \in \mathbb{R}^3$ is given by

the following:

$$\mathbf{r}_j = \mathbf{r}_{\text{cnt}} + A(\cos \theta_j \mathbf{r}_a + \sin \theta_j \mathbf{r}_b) + z_j \mathbf{r}_c, \quad (2)$$

$$\theta_j = \frac{2\pi}{N}(j-1), \quad (3)$$

where $j \in \{1, \dots, N\}$ is the index of the focus position, N is the total number of focus positions in one cycle of the LM, $\mathbf{r}_{\text{cnt}} \in \mathbb{R}^3$ is the center of the focal trajectory, and A is the radius of the trajectory. \mathbf{r}_a , \mathbf{r}_b , and \mathbf{r}_c are unit vectors whose origin is at \mathbf{r}_{cnt} and parallel to the x-, y-, and z-axis, respectively. The value of z_j was determined using the measured finger depth position. Based on these definitions, the step width of the focus movement is $d^{\text{LM}} = \frac{2\pi A}{N}$. The index of focus position j changes after the dwell time of focus t_d . Dwell time was $t_d = \frac{1}{N f^{\text{LM}}}$ if the frequency of the LM stimulus is f^{LM} .

Second, we formulated the LM-M stimulus. Let $\mathbf{r}_{i,j} \in \mathbb{R}^3$ be the focus position on the LM trajectory of the i -th focus among the foci presented simultaneously. $\mathbf{r}_{i,j}$ is chosen from \mathbf{r}_j , which is the position discretized with d^{LM} , such that the motion step width of the multi foci is fixed to d^{LM} . The conversion from \mathbf{r}_j to $\mathbf{r}_{i,j}$ is expressed as follows:

$$\mathbf{r}_{i,j} = \mathbf{r}_{j+(i-1)l}, \quad (4)$$

$$l = \left\lfloor \frac{d}{d^{\text{LM}}} \right\rfloor, \quad (5)$$

where l is the index number calculated from the distance between the multi foci d . l is an integer, and the decimal point is rounded down.

V. EXPERIMENTAL EQUIPMENT

In this section, we describe the experimental equipment that presents a midair image with noncontact tactile feedback. This equipment was used in all the subject experiments conducted in this study.

A. System Overview

Fig. 3 shows the experimental equipment and its coordinate system. This system consists of the four AUTDs, a midair image display (ELF-SR1 Spatial Reality Display, SONY), and a depth camera (RealSense D435, Intel) used to measure the finger position. In the experiments, we used the midair image display to instruct participants where to put their fingers. The coordinate system is a right-handed system whose origin is the center of the surface of the image display.

Throughout all the experiments, the system presented a 1×1 cm image marker at (0, 30, 30) mm. Ultrasound waves were output from the AUTDs when participants placed their fingertips on the marker. The presented ultrasound wave refracted on the surface of the image display and then focused on the finger pad. The position of the reflected ultrasound focus $\mathbf{r}_{\text{ref}} \in \mathbb{R}^3$ can be calculated as the mirror image of the original focus position $\mathbf{r}_{\text{org}} \in \mathbb{R}^3$ which is expressed as follows:

$$\mathbf{r}_{\text{ref}} = \mathbf{r}_{\text{org}} + 2((\mathbf{r}_p - \mathbf{r}_{\text{org}}) \cdot \mathbf{n})\mathbf{n}, \quad (6)$$

where \mathbf{n} is the normal vector of the display surface (reflective surface), and \mathbf{r}_{org} is an arbitrary point on the display surface.

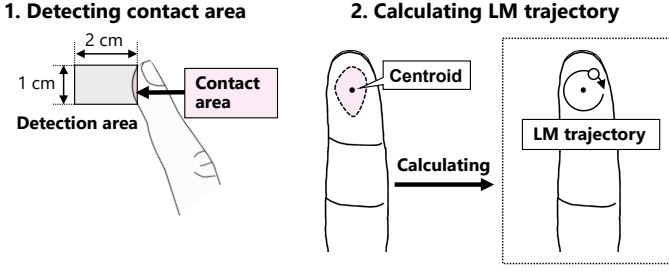


Fig. 4. Algorithm for presenting LM stimulus. The size of the detection area is $1 \times 1 \times 2$ cm. The part of the finger within this detection area is measured as the contact area, and the focal trajectory of the LM stimulus is calculated using this area. The center of the LM is the centroid of the contact area.

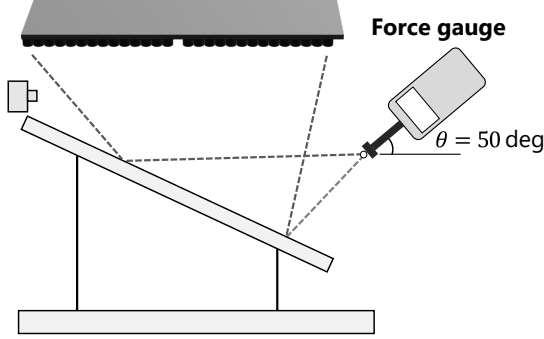


Fig. 5. Setup for measuring radiation force. The tip of the force gauge to which a 1.5 cm diameter acrylic disk was attached was placed at the focal point. The force gauge was tilted 50 deg so that this disk opposed the propagation direction of the ultrasound wave.

B. Algorithm for Presenting LM Stimulus

In the system, there are three processes for presenting a circular LM stimulus to the finger pad of the participant. Fig. 4 illustrates the presentation process. First, the system detects the contact area between a participant's finger and midair image marker using a depth camera. The size of the image marker is $1 \times 1 \times 0.5$ cm. However, to measure the contact position stably, we used the area from the surface of the image marker to 2 cm behind ($1 \times 1 \times 2$ cm) for the contact detection. Part of the finger within the detection area was measured as the contact area. Second, the system calculated the focal trajectory for the circular LM stimulus using eq. 2 or eq. 4. The center position of the LM stimulus r_{cnt} was the centroid of the detected contact area. The measured depth map of the fingertip surface was used for the z-position of the focal trajectory. Third, the focus is presented and moved along with the calculated trajectory at a pre-specified frequency. In this algorithm, the r_{cnt} is asynchronously updated with the focus position at 90 fps. A Gaussian filter was applied to the calculated r_{cnt} of 10 frames to suppress the measurement error of the depth camera.

C. Measurement of Radiation Force

We measured the radiation force of the focus presented by the system and it was 0.02 N. Fig. 5 shows the measurement setup. In this experiment, the tip of a force gauge, to which a 1.5 cm diameter acrylic disk was attached, was placed at the focal point. This force gauge (IMADA ZTS-2N) can measure forces up to 2 N with a resolution of 0.001 N. The force gauge

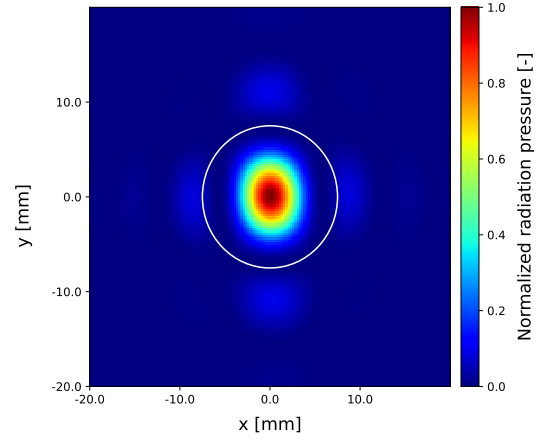


Fig. 6. Simulated radiation pressure distribution of focus. The white circle with a diameter of 1.5 cm means the area for measuring the radiation force.

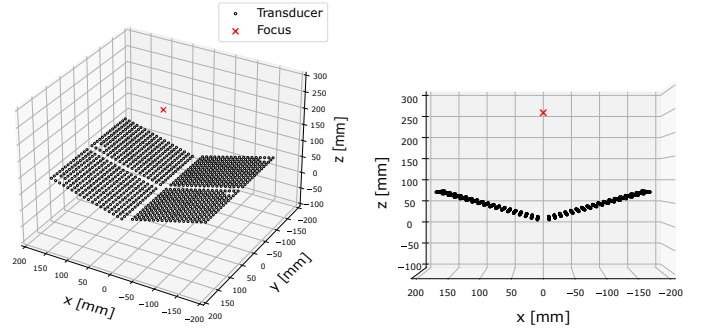


Fig. 7. AUTD setup for the simulation.

was tilted by 50 deg so that this disk opposes the propagation direction of the ultrasound wave. The size of the acrylic disk was determined based on the preliminary simulation such that the disk size was larger than the focus size. Fig. 6 shows the simulated radiation force distribution of a single focus and Fig. 7 shows the ultrasound transducer setup used for the simulation. The measurement range of the acrylic disk is superimposed on the simulated result as a white circle. In this simulation, the focus was generated at (0, 0, 250) mm, and the reflection of the sound waves was not considered. The focus position is shown in Fig. 7 as a cross mark.

VI. EXPERIMENT 1: STATIONARITY AND SURFACE CURVATURE

In this experiment, we evaluated the intensity of vibratory and movement sensations in the LM stimulus and the perceived curvature of the surface of the object produced by the LM same stimulus (i.e., flat, convex, or concave).

A. Stimulus Condition

In this experiment, we presented the LM-M (LM-multi foci) and LM-S (LM-single focus) stimuli at 5 Hz (as described in Section IV). For comparison, an LM-S stimulus at 25 Hz was also presented. The radii of LM stimuli A were 2, 3, 4, 5, and 6 mm. The motion step width d^{LM} of the LM stimulus at 5 Hz was as fine as 0.23 mm to elicit static pressure sensation [13].

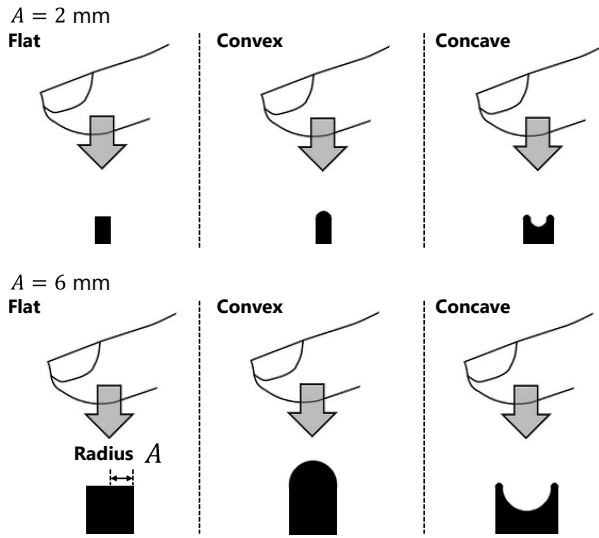


Fig. 8. Example of the presented picture to evaluate the perceived curvature ($A = 2, 6$ mm). The radius of the object was changed according to the radius of the presented LM stimulus A . For one stimulus condition, the image of flat, convex, and concave was sequentially presented in random order. Participants reported the perceptual similarity between the perceived curvature and the image.

Moreover, the step d^{LM} at 25 Hz was 4 mm to avoid exceeding the AUTD update limits (1 kHz) [33]. For the 5 Hz LM-M stimuli, the number of simultaneously presented foci N_{focus} was four, and their placement interval d was 3 mm. All stimuli were presented in random order. Each participant underwent two sets of experiments. Therefore, 30 experimental trials were conducted (i.e., 3 different LM stimuli \times 5 stimulus radii \times 2 sets = 30 experimental trials).

B. Procedure

Eight males (24–31 age) and two females (24 and 28 age) participated in this experiment.

The experimental equipment was a visuo-tactile display (Fig 3 and Section V). Participants were instructed to place their index fingertips on the presented midair image marker. The tactile stimulus was always presented while the fingertip was touching the marker.

First, to evaluate the tactile sensation of the presented stimulus, the participants answered the following two questions with a seven-point Likert scale:

- Q1. How intensely did you perceive a vibratory sensation in the presented stimulus?
- Q2. How intensely did you perceive the movement of the stimulus position?

Participants were instructed to answer 1 if they perceived no vibration or movement. In Q2, we evaluated whether the participants noticed the circular focus movement of the LM.

Second, the participants evaluated the curvature rendered by the LM stimulus on their finger pads. In this experiment, we provided three typical shapes as references (i.e., flat, convex, and concave). Three images corresponding to the three shapes (Fig. 8) were presented to the participants as reference images.

To evaluate the perceived curvature, the participants responded to Q3 with a seven-point Likert scale.

- Q3. Does the stimulus shape perceived at your finger pad match the situation illustrated in the reference images?

For one stimulus condition, flat, convex, and concave reference images (Fig. 8) were presented successively in random order. Participants independently reported perceptual similarity to each reference image (i.e., flat, convex, and concave). We varied the radius of the illustrated object in the reference images to match that of LM stimulus A .

Participants were instructed to ignore differences in the perceived size between the image and tactile stimulus to evaluate only the similarity of the perceived curvature (i.e., flat, convex, and concave). The overall size of the finger sketch, which was drawn in the reference image, was adjusted so that its nail size matches the average Japanese adult nail length (13.6 mm) [34].

C. Results and Analysis

1) *Stationarity*: Box-and-whisker plots of the evaluated vibratory sensations (answers to Q1) are shown in Fig. 9a. The evaluated movement sensation (answers to Q2) is also shown in Fig. 9b. If the data value v satisfies the following conditions, the data are treated as an outlier:

$$\begin{cases} v \leq v^{25} - 1.5 \times IQR, \\ v \geq v^{75} + 1.5 \times IQR, \end{cases} \quad (7)$$

where v^{25} and v^{75} are the 25-percentile value and 75-percentile value, respectively, and IQR is the interquartile range. Outliers were plotted as white dots in the graphs. As seven participants could not perceive the LM-M stimulus with $A = 2$ mm, their answers were excluded. In total, 13 data of the LM-M with $A = 2$ mm were excluded from each graph.

The results showed that the highest median value of the vibratory sensation score was 7, and the stimulus condition was LM-S at 25 Hz with $A = 4, 5, 6$ mm. The lowest median value was 1, and the condition was LM-M at 5 Hz with $A = 2$ mm. The highest median value of the movement sensation score was 6.5, and the stimulus condition was LM-S at 5 Hz with $A = 5$ mm. The lowest median value was 1, and the condition was LM-M at 5 Hz with $A = 2$ mm.

We conducted the Wilcoxon signed-rank test with Bonferroni correction to compare the results between the stimulus conditions (LM-M, LM-S at 5 Hz, and LM-S at 25 Hz) for each stimulus radius A . The results of the LM-M stimulus with $A = 2$ mm were excluded from the analysis. The test results showed that at all values of A , the perceived vibratory sensation of the LM-S at 25 Hz was significantly higher than that of the other LM stimuli ($p < 0.005$). At $A = 3$ mm, the vibratory sensation of the LM-S at 5 Hz was significantly higher than that of the LM-M ($p < 0.05$). The results also showed that at $A = 3, 4, 5, 6$ mm, the perceived movement sensation of the LM-S at 25 Hz was significantly lower than that of the other LM stimuli ($p < 0.05$). At $A = 3, 4, 5$ mm, the movement sensation of the LM-M was significantly lower than that of the LM-S at 5 Hz ($p < 0.05$). Fig. 9 shows these pairs with significant differences as "***" and "***" for $p < 0.05$ and $p < 0.005$, respectively.

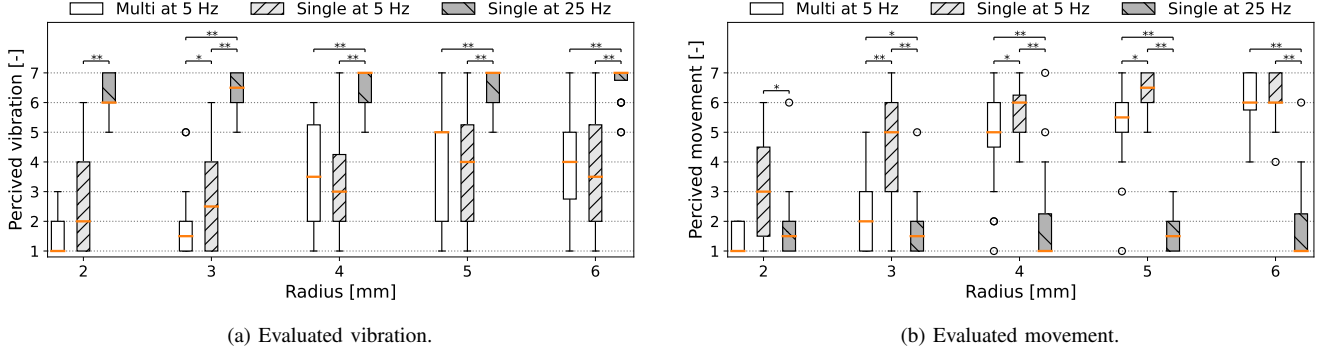


Fig. 9. Evaluated perceptual stationarity of LM stimulus on a finger pad in experiment 1. Participants evaluated the perceived intensity of the vibratory sensation and the focal movement sensation of the LM stimulus with a seven-point Likert scale.

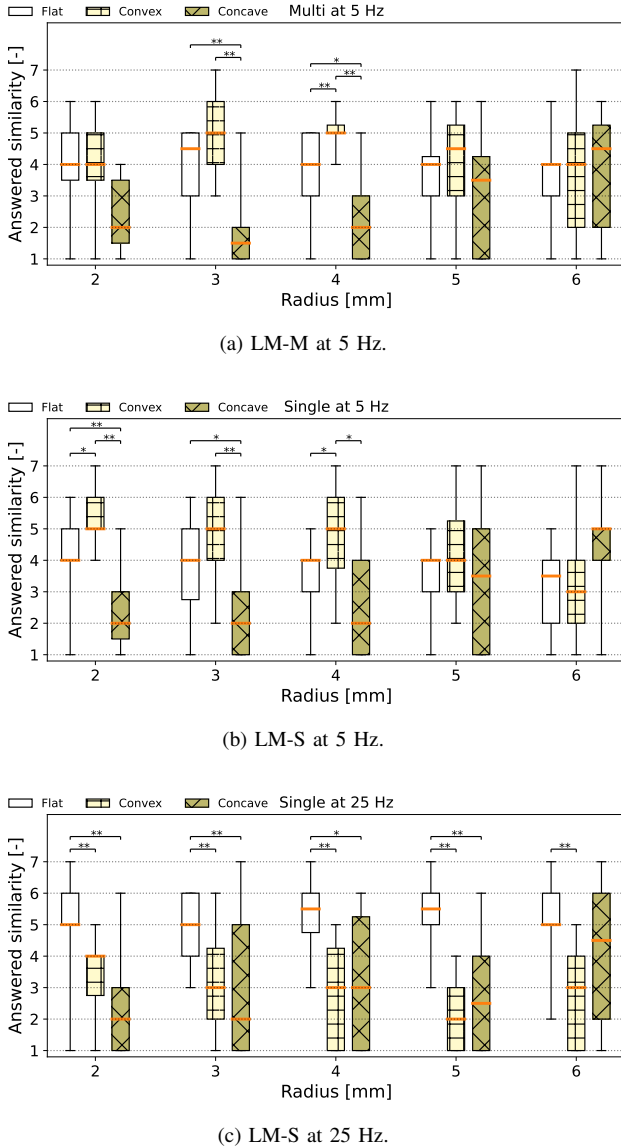


Fig. 10. Evaluated perceived curvature in experiment 1. The reference images with flat, convex, and concave was presented, and the participants answered perceptual similarity between the perceived tactile shape (curvature) and the image with a seven-point Likert scale.

Moreover, we conducted the Friedman test with Bonferroni correction using stimulus radius A and stimulus type (LM-M, LM-S at 5 Hz, and LM-S at 25 Hz) as factors. The test results showed that A and stimulus type had a significant effect on both vibration and movement sensation ($p < 0.0005$).

2) *Surface Curvature*: Box-and-whisker plots of the evaluated tactile shape (answers to Q3) with LM-M, LM-S at 5 Hz, and LM-S at 25 Hz are shown in Fig. 10a, Fig. 10b, Fig. 10c, respectively. 13 data of LM-M with $A = 2$ mm were excluded (Section VI-B).

The highest median value for the flat score was 5.5, and the condition was LM-S at 25 Hz with $A = 4, 5$ mm. The lowest median was 3.5, and the condition was LM-S at 5 Hz with $A = 6$ mm. The highest median for the convex score was 5, and the conditions were LM-M with $A = 3, 4$ mm and LM-S at 5 Hz with $A = 2, 3, 4$ mm. The lowest median was 2, and the condition was LM-S at 25 Hz with $A = 5$ mm. The highest median value of the concave score was 5, and the condition was LM-S at 5 Hz with $A = 6$ mm. The lowest median was 1.5, and the condition was LM-M with $A = 3$ mm.

We conducted the Wilcoxon signed-rank test with Bonferroni correction to compare the score between the shapes (i.e., flat, convex, concave) at each stimulus condition. The test result showed that in the LM-M with $A = 3, 4$ mm, the flat and convex scores were significantly higher than the concave scores ($p < 0.05$). With $A = 4$ mm, the convex score was significantly higher than the flat score ($p < 0.005$). In the LM-S at 5 Hz with $A = 2, 3$ mm, the flat score was significantly higher than the concave score ($p < 0.05$). For $A = 2, 3, 4$ mm, the convex score was significantly higher than the concave score ($p < 0.05$). With $A = 2$ mm, the convex score was also significantly higher than the flat score ($p < 0.05$). In the LM-S at 25 Hz, all flat scores were significantly higher than the convex scores ($p < 0.005$). For $A = 2, 3, 4, 5$ mm, the flat score was significantly higher than the concave score ($p < 0.05$).

VII. EXPERIMENT2: PERCEIVED SIZE

In this experiment, we changed the radius of LM stimulus A and evaluated the perceived stimulus size.

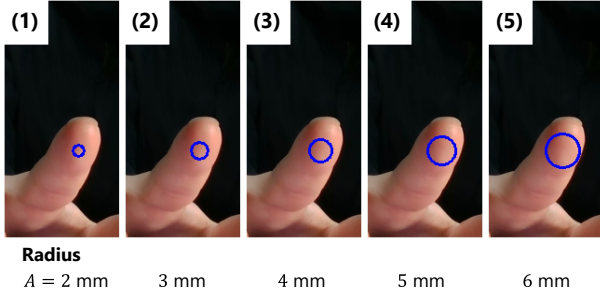


Fig. 11. Presented picture to evaluate the perceived size of the presented LM stimulus. The five pictures with different radii (2, 3, 4, 5, and 6 mm) were presented simultaneously. Participants selected one of these images showing the circle whose size matches the perceived haptic size.

A. Procedure

Eight males (24–31 age) and (24 and 28 age) two females participated in this experiment.

The experimental setup was the same as that used in Experiment 1 (Fig. 3). The tactile stimulus was always presented while the fingertip was touching the marker. The stimulus conditions were identical to those used in Experiment 1, which is explained in Section VI-A. 30 experimental trials were conducted (i.e., 3 different LM stimuli \times 5 stimulus radii \times 2 sets = 30 experimental trials).

A real-time video of the participants' fingers was presented to them during the experiment. The screenshot of the presented video is shown in Fig. 11. In this video, a blue circular image corresponding to the trajectory of the LM stimulus is superimposed on the finger pad of the participant. Participants selected one of the videos showing a circle whose size matched the perceived haptic size to evaluate the perceived size of the presented stimulus.

The center of the circular image was changed in real-time to match the center of the presented LM stimulus r_{cnt} . The radii of the circular images were 2, 3, 4, 5, and 6 mm, which were the same as the radii of LM stimuli A used in this experiment. Five videos with different radii were simultaneously presented to the participant. This video was captured using an RGB camera built into the depth camera.

B. Results and Analysis

Fig. 12 presents the confusion matrix for the stimulus size identification results. The highest accuracy was 0.6, and the stimulus condition was LM-S at 5 Hz with $A = 5$ mm. The lowest accuracy was 0.15, and the condition was LM-S at 25 Hz with $A = 2, 4$ mm. Chance rate in this experiment was 0.2, and accuracy exceeded the chance rate in all conditions, except for the lowest-accuracy condition.

We compared the perceived size across the stimulus condition (LM-M and LM-S at 5 Hz and 25 Hz, respectively). Fig. 13 shows box-and-whisker plots of the perceived stimulus sizes. The highest perceived stimulus radius was 5 mm, and the condition was LM-S at 5 and 25 Hz with $A = 5$ mm and all LM stimuli with $A = 6$ mm. The lowest radius was 2 mm, and the conditions were LM-M with $A = 2, 3$ mm.

We applied the Wilcoxon signed-rank test with Bonferroni correction to the results of the perceived size. The test results

showed that the perceived radii of the LM-S at 25 Hz were significantly higher than that of the LM-M with $A = 3, 4, 5$ ($p < 0.05$) and LM-S at 5 Hz with $A = 2, 4, 5$ mm ($p < 0.05$). The results also showed that the radius of the LM-S at 5 Hz was significantly larger than that of the LM-M with $A = 3, 4$ mm ($p < 0.05$).

VIII. EXPERIMENT3: EQUIVALENT PHYSICAL STIMULUS

This experiment investigated physically static force which is equivalent to the pressure sensation evoked by LM stimulus at a finger pad. Physical force was presented by pushing a force gauge against the finger pad.

A. Setup and Stimulus

Fig. 14 illustrated the experimental setup. In this experiment, we used a force gauge whose z-position was automatically controlled by a 3-axis stage (QT-AMM3 and ALS-7013-G1MR, CHUO PRECISION INDUSTRIAL Co., Ltd.) and the visual-haptic system (Fig. 3) used in the other experiments. This force gauge (IMADA ZTS-50N) can measure forces up to 50 N with a resolution of 0.01 N. The stimulus condition was the same as that used in Experiment 1, which is explained in Section VI-A.

There were 30 experimental trials conducted (3 different LM stimuli \times 5 stimulus radii $A \times$ 2 sets = 30 experimental trials).

B. Procedure

Eight males (23–28 age) and two females (24 and 28 age) participated in this experiment.

Participants were instructed to place their index fingers of their right hands on the marker presented by the midair image display. Participants were also instructed to place their index fingers of their left hands such that the finger pad faced the tip of the force gauge. At this point, the force gauge did not touch the finger pad. The force gauge was fixed in midair in a horizontal orientation (Fig. 14). Participants grasped the aluminum handle and fixed their finger position by placing it in front of an acrylic auxiliary plate. A plastic cylinder with a radius of 1 cm was attached to the tip of the force gauge. The basal plane of the cylinder was beveled to 1 mm so that the participants did not perceive its edges. Participants wore headphones and listened to white noise during the experiment to avoid hearing the driving noise of the AUTD.

A force gauge was pressed against the finger pad of the participant by moving along the z-axis. After the force gauge reached the specified position (the initial pushing depth was 4 mm), an LM stimulus was presented to the finger pad of the right hand. After 2 s, the LM stimulus was stopped, and the force gauge returned to its initial position. The force gauge immediately started pushing again, and the LM stimulus was presented again. This 2 s tactile stimulation was repeated automatically. In this experimental loop, participants compared the physical pushing force with the LM stimulus and orally reported the results. Based on the participants' answers, we changed the pushing depth of the force gauge such that the

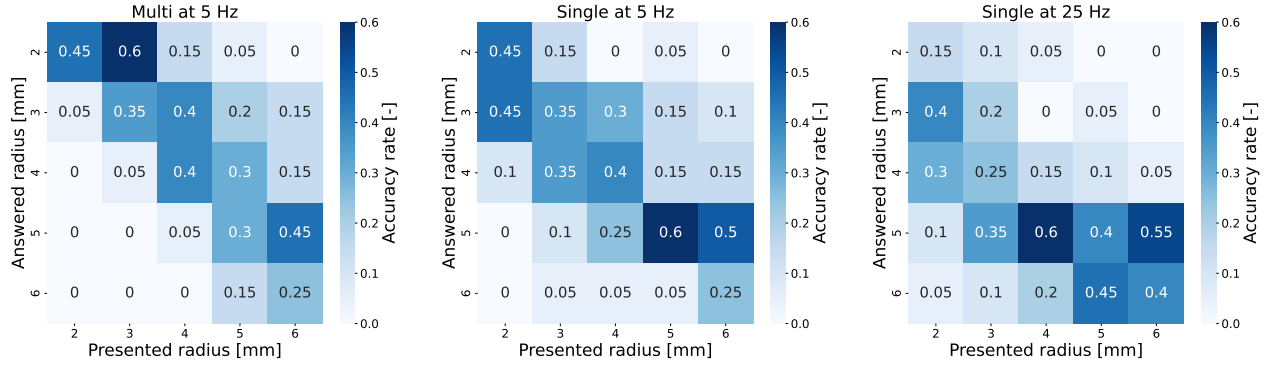


Fig. 12. Confusion matrix of the stimulus size identification. The chance rate in this experiment was 0.2.

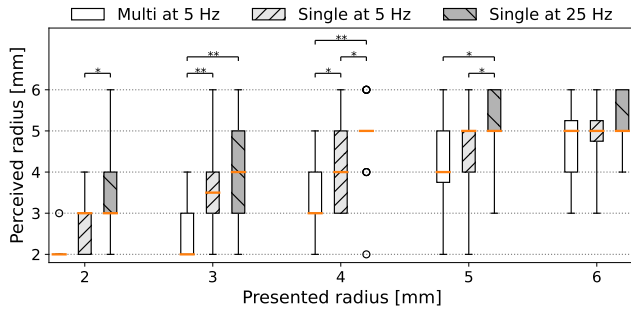


Fig. 13. Evaluation result of the perceived size of the circular LM stimulus.

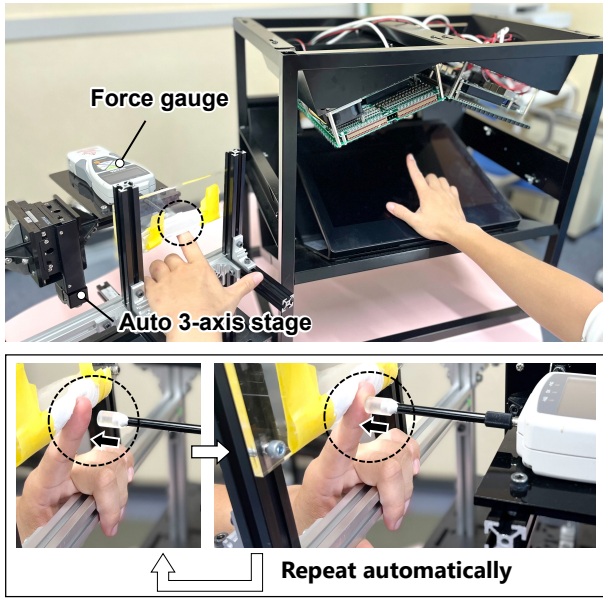


Fig. 14. Setup to evaluate the perceived force. A force gauge was pressed against the finger pad of the left hand, and the LM stimulus was presented to the right finger. The pushing depth was automatically controlled by the 3-axis stage. These stimuli were terminated after 2 s and automatically repeated. Participants compared the pushing force with the LM stimulus and orally reported the comparison results.

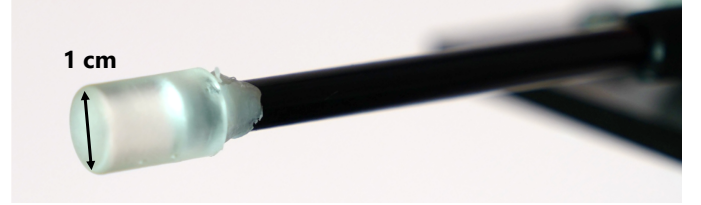


Fig. 15. Plastic cylinder attached to the tip of the force gauge, used to push a finger pad. The radius was 1 cm, and the basal plane of the cylinder was beveled 1 mm.

perceived intensity of the two stimuli is the same. For example, pushing depth in the 2nd stimulus was shortened to weaken the pushing force if the participant answered that the pushing force was stronger than the LM stimulus in the 1st stimulus. The force gauge kept pushing the finger pad and recorded the pushing force for 2 s when the participants reported that the intensities of the two stimuli were the same. The median value of the pushing force time series data was finally adopted as the measured force. After the measurement, the stimulus conditions were changed, and the same procedure was repeated. The adjustment resolution of the pushing depth is 0.25 mm and the speed of the force gauge was 5 mm/s. The maximum number of pushing depth adjustments was 20, and all participants completed the experiment within 30 min.

In the stimulus comparison, we instructed the participants to ignore the perception at the moment when the LM stimulus and the pushing force were presented to assess the steady-state perceived intensity of the LM stimulus.

C. Results and Analysis

In this experiment, the median value of the measured force time series data was adopted as the participant's answer. The maximum standard deviation (SD) of the time series data, median value, and minimum values were 0.522, 0.186, and 0, respectively. The maximum, median, and minimum values were answered by a different participant. Fig. 16 shows the times series data whose SD is the maximum (0.522) and data whose SD is the median (0.186). The median force of each time series data is shown in Fig. 16 as a red line.

Fig. 17 shows the box-and-whisker plots of the pushing forces. Outliers were calculated using eq. 7, and are plotted

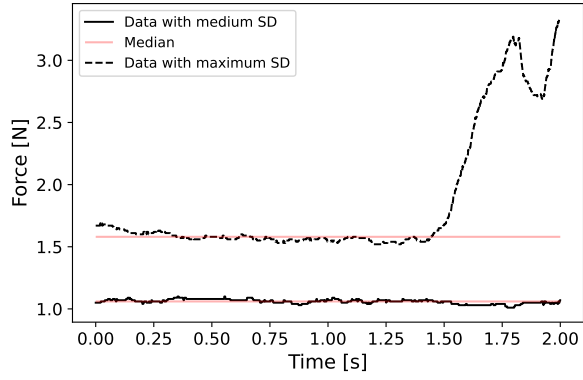


Fig. 16. Time series data of measured force. We calculated the standard deviation (SD) of each recorded time series data, and the data with the maximum SD (0.522) and with the median value of the SD (0.186) was plotted in this figure. We also plotted the median value of these plotted time series force.

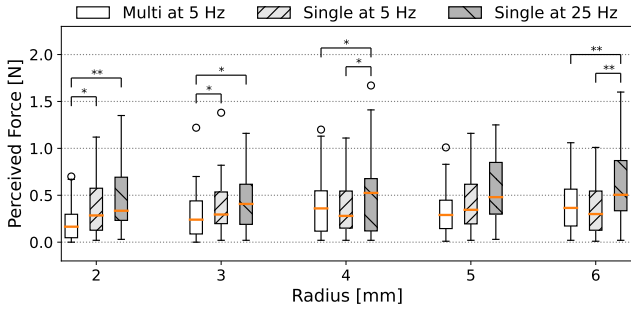


Fig. 17. Physically static pushing force perceptually equal to the intensity of the LM stimulus.

as white dots. One participant was unable to perceive the LM at 5 Hz with $A = 2$ mm; thus, this value was plotted as 0 N. The forces lower than 0.01 N, which is the lowest measurable force of the force gauge, were also plotted as 0 N. The results showed that the highest median value of the perceived force was 0.53 N, and the stimulus condition was LM-S at 25 Hz with $A = 4$ mm. The lowest median value was 0.16 N, and the condition was LM-M at 5 Hz with $A = 2$ mm.

We also conducted the Wilcoxon signed-rank test with Bonferroni correction to compare the perceived force between the stimulus conditions (LM-M, LM-S at 5 Hz, and LM-S at 25 Hz) at each stimulus radius A . The test results showed that with $A = 2, 3, 4, 6$ mm, the perceived force of the LM-S stimulus at 25 Hz was significantly higher than that of the LM-M stimulus ($p < 0.05$). For $A = 4, 6$ mm, the perceived force of the LM-S stimulus at 25 Hz was significantly higher than that of the LM-S stimulus at 5 Hz ($p < 0.05$). For $A = 2, 3$ mm, the perceived force of the LM-S stimulus at 5 Hz was significantly higher than that of the LM-M stimulus ($p < 0.05$).

IX. DISCUSSION

A. Static Pressure Sensation at Finger Pad

The results of Experiment 1 showed that LM at 5 Hz (including both LM-M and LM-S) can produce a non-vibratory

pressure sensation on a finger pad. Moreover, with stimulus radii of $A = 2, 3$ mm, the movement sensations were barely perceivable, and the pressure sensation was well static. The vibration sensation of the LM stimulus at 5 Hz was 4 or less in all conditions except LM-M with $A = 5$ mm, which was significantly lower than that of the LM-S at 25 Hz. For $A = 2, 3$, the movement sensations of the LM-M were 2 or less.

The results of Experiment 3 also showed that the perceived intensity of the pressure sensation on the finger pad was perceptually comparable to 0.16 N or more physical contact force on average. With the lowest vibration and movement sensation (LM-M with $A = 3$ mm), the perceived force was 0.24 N, which was 12 times the radiation pressure at the focus presented in the setup.

However, in Experiment 3, extremely low and high forces were identified causing large variance. For the LM-M with $A = 3$ mm, the minimum and maximum values were 0 and 1.22 N, respectively. Note that the participant who answered 0 N could perceive the LM-M stimulus with $A = 3$ mm. Since the answered equivalent force is less than 0.01 N, which is the measurable minimum force of the force gauge, the force is recorded as 0 N. This large difference in perceived force could be attributed to the individual differences in the tactile receptor-adaptation speed to the pushing stimulus presented by the force gauge. The pushing force is static, and the perceived intensity of such stimulus gradually weakens with stimulus duration owing to SA-I (slowly-adaptive type I) tactile receptor adaptation [35]. In Experiment 3, the contact time with the force gauge was controlled for 2 s to prevent this adaptation effect, and participants were instructed to ignore the perception of the moment of the contact. However, if the adaptation speed greatly differs among participants, even under this control, there could be a large difference in the answered equivalent pushing force. For example, we considered that the adaptation speed of the participants answered an extremely high force was fast. When the adaptation speed is fast, the perceived intensity of the contact force rapidly weakens over the period of 2 s, resulting in a high pushing force as the equivalent force. Conversely, the adaptation speed of the participants answering an extremely low force could be slow. The evaluation of the individual differences in adaptation speed is important for future work.

The experimental results also indicated that the perceived intensity of the LM-M stimulus with $A = 2$ mm was extremely weak. In Experiments 1 and 2, eight participants could not perceive the LM-M stimulus with $A = 2$ mm. We considered that the weakness is because the circumference with a 2 mm radius and the length of the curved line-shaped stimulus distribution used in LM-M (9 mm) were almost the same. As an exception, in Experiment 3, only one participant could not perceive the LM-M stimulus with $A = 2$ mm, and the average perceived force was 0.16 N. This difference could be attributed to the difference in the presentation time of the LM stimulus [35]. In Experiment 3, the stimulus duration was 2 s, but in Experiments 1 and 2, the participants continued to be presented with the LM stimulus without any time limit. Therefore, in most participants in Experiments 1 and 2,

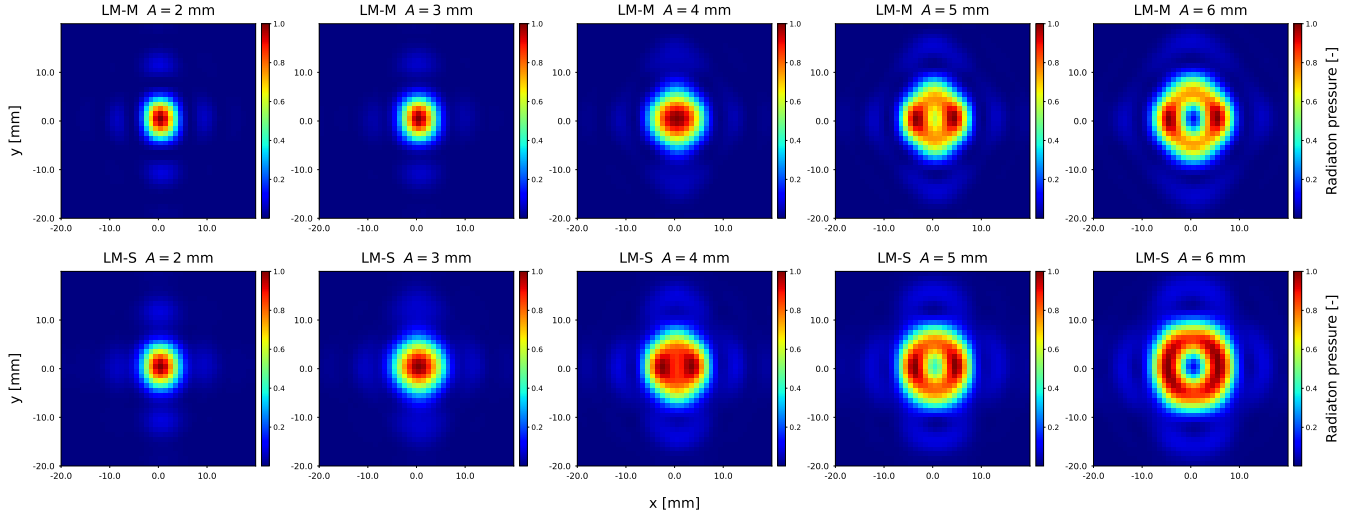


Fig. 18. Simulated time-averaged radiation pressure distribution. These values were normalized.

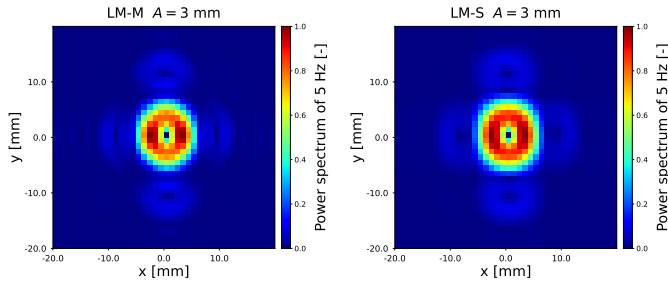


Fig. 19. Simulated 5 Hz-power spectrum distribution of time variation of radiation pressure produced by LM-M and LM-S at 5 Hz. The power spectrum distribution was obtained by simulating the time variation of the radiation pressure at each point in the stimulus area and Fourier transforming the time variation. These values were normalized.

their SA-I tactile receptors completely adapted to the LM-M stimulus, and they could not perceive the stimulus.

B. Perceived Curvature

In Experiments 1 and 2, since eight participants could not perceive the LM-M stimulus with a radius of 2 mm, we excluded it from the following discussions.

The results of Experiments 1 and 2 suggest that a circular LM stimulus with $A = 2\text{--}4$ mm can render a contact sensation with a convex surface with radii of 2–4 mm. As described in Section IX-A, particularly for the $A = 2, 3$ mm, the contact sensation was well static. In the LM at 5 Hz with $A = 2\text{--}4$ mm, the convex score was significantly higher than the concave score ($p < 0.05$). In LM-M with $A = 4$ mm and LM-S with $A = 2, 4$ mm, the convex score was significantly higher than the flat score ($p < 0.05$). The perceived radii for LM-M with $A = 3$ mm and LM-S with $A = 4$ mm were 2 and 4, respectively. The comments of participants also suggest that convex sensation was rendered. Four participants commented that they sometimes felt in contact with sharp or rounded objects. Based on the authors' subjective view, we felt the LM-M and LM-S stimuli at 5 Hz with $A = 3$ mm as a contact sensation with a rounded convex surface.

However, in some cases, participants found it difficult to determine whether the perceived contact shape was convex or flat. Two of the participants commented that this determination was difficult. Moreover, no significant differences were observed between the convex scores for the LM-S at 5 Hz with $A = 3$ mm and LM-M with $A = 3$ mm. In the future, we will quantitatively evaluate the curvature of the perceived surface and explore a control method for the curvature.

In the LM at 5 Hz with $A = 2\text{--}4$ mm, all concave scores were less than 2, and a concave sensation was not perceived. We considered that the periphery of the LM was hardly perceived in the radius range as three participants commented that they had high concave scores when they strongly perceived the perimeter of the stimulus. The characteristics of the time-averaged radiation pressure distribution of the LM stimulus were also consistent with this consideration. Fig. 18 shows the simulated time-averaged pressure distribution. The simulation setup is the same that shown in Fig. 7. The results indicates that the periphery of the LM stimulus is the peak of the time-averaged radiation pressure only above a radius of 5 mm, where the concave score is high.

Finally, we compared the perceived curvature to the 5 Hz-vibration intensity distribution produced by the LM stimulus at 5 Hz. Fig. 19 shows the simulated distribution of the 5 Hz vibration intensity (power spectrum of 5 Hz) produced by LM-M and LM-S at 5 Hz with $A = 3$ mm. The power spectrum distribution was obtained by simulating the time variation of the radiation pressure at each point in the stimulus area and Fourier transforming the time variation. The simulation setup is the same that shown in Fig. 7. The simulation results showed that the physical intensity of the 5 Hz vibration was the highest on the focal orbits and does not match the perceived stimulus shape (perceived curvature). With $A = 3$ mm, the LM-M and LM-S at 5 Hz were perceived as contact with a convex surface. However, even under these conditions, the peaks of vibration intensity formed a circle, which is a contact shape with concave. In the future, we will investigate the relationship between perceived curvature and vibration intensity distribu-

tion by measuring or simulating skin displacement generated by the LM stimulus as in previous studies [36], [37].

C. Comparison of LM-M and LM-S at 5 Hz

The results of Experiment 1 showed that the curved line-shaped pressure distribution, which consists of four ultrasound foci and is used in LM-M, can suppress the movement sensation of low-frequency LM stimuli. With $A = 3, 4, 5$, the movement sensation of the LM-M was significantly lower than that of the LM-S at 5 Hz. We considered that the reason for the suppression of motion perception was that the simultaneously stimulated area of LM-M was wider than that of LM-S.

The LM-M stimulus was perceived to be smaller than the LM-S stimulus at 5 Hz. For $A = 3, 4$ mm, the perceived size of LM-M was significantly smaller than that of LM-S at 5 Hz ($p < 0.05$). The trend in perceived size is consistent with the difference in the size of the time-averaged radiation pressure distribution. The simulation results shown in Fig. 18 indicate that the time-averaged distributions of LM-M with $A = 3, 4$ mm were smaller than those of LM-S.

In terms of vibratory sensation and perceived shape (curvature), there were no huge differences between LM-M and LM-S at 5 Hz. Except for $A = 3$ mm, there were no significant differences in vibration sensations. For $A = 3, 4, 5$ mm, the convex scores were higher than the flat and concave scores for both the LM-M and LM-S at 5 Hz.

D. Comparison of Movement Sense Between LM Frequencies

The results of Experiment 1 showed that the movement sensation of the LM at 25 Hz was lower than that of the LM at 5 Hz. At $A = 3, 4, 5, 6$ mm, the movement sensation of the LM-S at 25 Hz was significantly lower than that of LM-M and LM-S at 5 Hz. We considered that this was because the focus speed at $f^{LM} = 25$ Hz was too fast for the participants to perceive movement different from the vibration. This result consisted with the previous study [38]. They presented circular STM stimuli with a diameter of 4–7 cm on the palm and found that the focal movement can not be perceived when the movement speed of the focus was above 18 Hz.

The results also showed that rendering a convex surface was difficult with the vibratory sensation produced by focused ultrasound. As the vibration score of LM-S at 25 Hz was 6 or higher, this stimulus evoked a vibratory sensation in the experiments. In the LM at 25 Hz, the flat score is the highest for all radii and was significantly greater than the convex score. One participant commented that the contact shape often felt flat when vibration was perceived.

X. CONCLUSION

In this study, we verified that ultrasound radiation pressure distribution, which spatiotemporally varies at 5 Hz, can provide a static pressure sensation on a finger pad. We also demonstrated that the pressure sensation on the finger pad was perceived as a static contact sensation with a convex surface. In the experiment, four ultrasound focal points were presented on the finger pads of the participant and they were simultaneously

rotated in a circle at 5 Hz. When the radius of the focal trajectory was 3 mm, the perceived vibration and movement sensations were the lowest, 1.5 and 2 out of 7 on average, respectively. The perceived intensity of this evoked pressure sensation was equivalent to a 0.24 N physically constant force lasting for 2 s, which is 12 times the physically presented radiation force at the focus. Under the most static condition, the pressure sensation was perceived as a contact sensation on a convex surface with a radius of 2 mm. The average perceptual similarity was 5 out of 7.

From these results, we conclude that focused ultrasound can render a static contact sensation at a finger pad with a small convex surface. This contact sensation rendering enables the noncontact tactile reproduction of a static-fine uneven surface. In the future, we will investigate curvature control of the rendered convex surface.

REFERENCES

- [1] I. Rakkolainen, E. Freeman, A. Sand, R. Raisamo, and S. Brewster, "A survey of mid-air ultrasound haptics and its applications," *IEEE Transactions on Haptics*, 2020.
- [2] T. Iwamoto and H. Shinoda, "Ultrasound tactile display for stress field reproduction-examination of non-vibratory tactile apparent movement," in *First Joint Eurohaptics Conference and Symposium on Haptic Interfaces for Virtual Environment and Teleoperator Systems. World Haptics Conference*. IEEE, 2005, pp. 220–228.
- [3] T. Hoshi, M. Takahashi, T. Iwamoto, and H. Shinoda, "Noncontact tactile display based on radiation pressure of airborne ultrasound," *IEEE Transactions on Haptics*, vol. 3, no. 3, pp. 155–165, 2010.
- [4] T. Carter, S. A. Seah, B. Long, B. Drinkwater, and S. Subramanian, "Ultrahaptics: multi-point mid-air haptic feedback for touch surfaces," in *Proceedings of the 26th annual ACM symposium on User interface software and technology*. ACM, 2013, pp. 505–514.
- [5] K. Yosioka and Y. Kawasima, "Acoustic radiation pressure on a compressible sphere," *Acta Acustica united with Acustica*, vol. 5, no. 3, pp. 167–173, 1955.
- [6] S. Suzuki, M. Fujiwara, Y. Makino, and H. Shinoda, "Midair hand guidance by an ultrasound virtual handrail," in *2019 IEEE World Haptics Conference (WHC)*. IEEE, 2019, pp. 271–276.
- [7] A. Yoshimoto, K. Hasegawa, Y. Makino, and H. Shinoda, "Midair haptic pursuit," *IEEE transactions on haptics*, vol. 12, no. 4, pp. 652–657, 2019.
- [8] E. Freeman, D.-B. Vo, and S. Brewster, "Haptiglow: Helping users position their hands for better mid-air gestures and ultrasound haptic feedback," in *2019 IEEE World Haptics Conference (WHC)*. IEEE, 2019, pp. 289–294.
- [9] Y. Monnai, K. Hasegawa, M. Fujiwara, K. Yoshino, S. Inoue, and H. Shinoda, "Haptomime: mid-air haptic interaction with a floating virtual screen," in *Proceedings of the 27th annual ACM symposium on User interface software and technology*, 2014, pp. 663–667.
- [10] T. Romanus, S. Frish, M. Maksymenko, W. Frier, L. Corenthy, and O. Georgiou, "Mid-air haptic bio-holograms in mixed reality," in *2019 IEEE international symposium on mixed and augmented reality adjunct (ISMAR-Adjunct)*. IEEE, 2019, pp. 348–352.
- [11] T. Morisaki, M. Fujiwara, Y. Makino, and H. Shinoda, "Midair haptic-optic display with multi-tactile texture based on presenting vibration and pressure sensation by ultrasound," in *SIGGRAPH Asia 2021 Emerging Technologies*, 2021, pp. 1–2.
- [12] Y. Makino, Y. Furuyama, S. Inoue, and H. Shinoda, "Haptoclone (haptic-optical clone) for mutual tele-environment by real-time 3d image transfer with midair force feedback," in *CHI*, 2016, pp. 1980–1990.
- [13] T. Morisaki, M. Fujiwara, Y. Makino, and H. Shinoda, "Non-vibratory pressure sensation produced by ultrasound focus moving laterally and repetitively with fine spatial step width," *IEEE Transactions on Haptics*, vol. 15, no. 2, pp. 441–450, 2021.
- [14] R. S. Johansson and Å. B. Vallbo, "Tactile sensory coding in the glabrous skin of the human hand," *Trends in neurosciences*, vol. 6, pp. 27–32, 1983.
- [15] S. J. Bolanowski Jr, G. A. Gescheider, R. T. Verrillo, and C. M. Checkosky, "Four channels mediate the mechanical aspects of touch," *The Journal of the Acoustical society of America*, vol. 84, no. 5, pp. 1680–1694, 1988.

- [16] K. Hasegawa and H. Shinoda, "Aerial vibrotactile display based on multi-unit ultrasound phased array," *IEEE transactions on haptics*, vol. 11, no. 3, pp. 367–377, 2018.
- [17] R. Takahashi, K. Hasegawa, and H. Shinoda, "Lateral modulation of midair ultrasound focus for intensified vibrotactile stimuli," in *International Conference on Human Haptic Sensing and Touch Enabled Computer Applications*. Springer, 2018, pp. 276–288.
- [18] —, "Tactile stimulation by repetitive lateral movement of midair ultrasound focus," *IEEE transactions on haptics*, vol. 13, no. 2, pp. 334–342, 2019.
- [19] W. Frier, D. Ablart, J. Chilles, B. Long, M. Giordano, M. Obrist, and S. Subramanian, "Using spatiotemporal modulation to draw tactile patterns in mid-air," in *International Conference on Human Haptic Sensing and Touch Enabled Computer Applications*. Springer, 2018, pp. 270–281.
- [20] T. Howard, G. Gallagher, A. Lécuyer, C. Pacchierotti, and M. Marchal, "Investigating the recognition of local shapes using mid-air ultrasound haptics," in *2019 IEEE World Haptics Conference (WHC)*. IEEE, 2019, pp. 503–508.
- [21] Z. Somei, T. Morisaki, Y. Toide, M. Fujiwara, Y. Makino, and H. Shinoda, "Spatial resolution of mesoscopic shapes presented by airborne ultrasound," in *International Conference on Human Haptic Sensing and Touch Enabled Computer Applications*. Springer, 2022, pp. 243–251.
- [22] W. Frier, D. Pittera, D. Ablart, M. Obrist, and S. Subramanian, "Sampling strategy for ultrasonic mid-air haptics," in *Proceedings of the 2019 CHI Conference on Human Factors in Computing Systems*, 2019, pp. 1–11.
- [23] G. Korres and M. Eid, "Haptogram: Ultrasonic point-cloud tactile stimulation," *IEEE Access*, vol. 4, pp. 7758–7769, 2016.
- [24] D. Hajas, D. Pittera, A. Nasce, O. Georgiou, and M. Obrist, "Mid-air haptic rendering of 2d geometric shapes with a dynamic tactile pointer," *IEEE transactions on haptics*, vol. 13, no. 4, pp. 806–817, 2020.
- [25] P. Marti, O. Parlangeli, A. Recupero, S. Guidi, and M. Sirizzotti, "Mid-air haptics for shape recognition of virtual objects," *Ergonomics*, pp. 1–19, 2021.
- [26] L. Mulot, G. Gicquel, Q. Zanini, W. Frier, M. Marchal, C. Pacchierotti, and T. Howard, "Dolphin: A framework for the design and perceptual evaluation of ultrasound mid-air haptic stimuli," in *ACM Symposium on Applied Perception 2021*, 2021, pp. 1–10.
- [27] L. Mulot, G. Gicquel, W. Frier, M. Marchal, C. Pacchierotti, and T. Howard, "Curvature discrimination for dynamic ultrasound mid-air haptic stimuli," in *2021 IEEE World Haptics Conference (WHC)*. IEEE, 2021, pp. 1145–1145.
- [28] S. Inoue, Y. Makino, and H. Shinoda, "Active touch perception produced by airborne ultrasonic haptic hologram," in *2015 IEEE World Haptics Conference (WHC)*. IEEE, 2015, pp. 362–367.
- [29] B. Long, S. A. Seah, T. Carter, and S. Subramanian, "Rendering volumetric haptic shapes in mid-air using ultrasound," *ACM Transactions on Graphics (TOG)*, vol. 33, no. 6, pp. 1–10, 2014.
- [30] A. Matsubayashi, Y. Makino, and H. Shinoda, "Direct finger manipulation of 3d object image with ultrasound haptic feedback," in *Proceedings of the 2019 CHI Conference on Human Factors in Computing Systems*, 2019, pp. 1–11.
- [31] A. Matsubayashi, H. Oikawa, S. Mizutani, Y. Makino, and H. Shinoda, "Display of haptic shape using ultrasound pressure distribution forming cross-sectional shape," in *2019 IEEE World Haptics Conference (WHC)*. IEEE, 2019, pp. 419–424.
- [32] S. Inoue, Y. Makino, and H. Shinoda, "Scalable architecture for airborne ultrasound tactile display," in *International AsiaHaptics conference*. Springer, 2016, pp. 99–103.
- [33] S. Suzuki, S. Inoue, M. Fujiwara, Y. Makino, and H. Shinoda, "Autd3: Scalable airborne ultrasound tactile display," *IEEE Transactions on Haptics*, 2021.
- [34] N. I. of Advanced Industrial Science and Technology, "Icam: Identification code of anthropometric measurements," 2011, <https://www.airc.aist.go.jp/dhrt/hand/data/list.html>.
- [35] A. B. Vallbo, R. S. Johansson *et al.*, "Properties of cutaneous mechanoreceptors in the human hand related to touch sensation," *Hum neurobiol*, vol. 3, no. 1, pp. 3–14, 1984.
- [36] J. Chilles, W. Frier, A. Abdouni, M. Giordano, and O. Georgiou, "Laser doppler vibrometry and fem simulations of ultrasonic mid-air haptics," in *2019 IEEE World Haptics Conference (WHC)*. IEEE, 2019, pp. 259–264.
- [37] W. Frier, A. Abdouni, D. Pittera, O. Georgiou, and R. Malkin, "Simulating airborne ultrasound vibrations in human skin for haptic applications," *IEEE Access*, vol. 10, pp. 15 443–15 456, 2022.

- [38] E. Freeman and G. Wilson, "Perception of ultrasound haptic focal point motion," in *Proceedings of the 2021 International Conference on Multimodal Interaction*, 2021, pp. 697–701.



Tao Morisaki Tao Morisaki is a Ph.D. student with the Graduate School of Frontier Sciences, the University of Tokyo, since 2020. He received the M.S. degree from the Department of Complexity Science and Engineering from the University of Tokyo, Chiba, Japan, in 2020. His research interests include haptics, ultrasound midair haptics, and human-computer interaction. He is a member of VRSJ.



Masahiro Fujiwara He is a project assistant professor in the Graduate School of Frontier Sciences, the University of Tokyo, Japan. He received the BS degree in Engineering, the MS degree and the PhD degree in Information Science and Technology from the University of Tokyo, in 2010, 2012, and 2015, respectively. His research interests include information physics, haptics, non-contact sensing and application systems related to them. He is a member of IEEE.



Yasutoshi Makino Yasutoshi Makino is an associate professor in the Department of Complexity Science and Engineering in the University of Tokyo. He received his PhD in Information Science and Technology from the Univ. of Tokyo in 2007. He worked as a researcher for two years in the Univ. of Tokyo and an assistant professor in Keio University from 2009 to 2013. From 2013 he moved to the Univ. of Tokyo as a lecture, and he is an associate professor from 2017. His research interest includes haptic interactive systems.



Hiroyuki Shinoda Hiroyuki Shinoda is a Professor at the Graduate School of Frontier Sciences, the University of Tokyo. After receiving a Ph.D. in engineering from the University of Tokyo, he was an Associate Professor at Tokyo University of Agriculture and Technology from 1995 to 1999. He was a Visiting Scholar at UC Berkeley in 1999 and was an Associate Professor at the University of Tokyo from 2000 to 2012. His research interests include information physics, haptics, mid-air haptics, two-dimensional communication, and their application systems. He is a member of SICE, IEEJ, RSJ, JSME, VRSJ, IEEE and ACM.